

## Inertial modes of a periodically forced buoyant drop attached to a capillary

Nicolas Abi Chebel, Frédéric Risso, and Olivier Masbernat

Citation: *Phys. Fluids* **23**, 102104 (2011); doi: 10.1063/1.3646930

View online: <http://dx.doi.org/10.1063/1.3646930>

View Table of Contents: <http://pof.aip.org/resource/1/PHFLE6/v23/i10>

Published by the AIP Publishing LLC.

---

### Additional information on Phys. Fluids

Journal Homepage: <http://pof.aip.org/>

Journal Information: [http://pof.aip.org/about/about\\_the\\_journal](http://pof.aip.org/about/about_the_journal)

Top downloads: [http://pof.aip.org/features/most\\_downloaded](http://pof.aip.org/features/most_downloaded)

Information for Authors: <http://pof.aip.org/authors>

### ADVERTISEMENT



**Running in Circles Looking  
for the Best Science Job?**

Search hundreds of exciting  
new jobs each month!

<http://careers.physicstoday.org/jobs>

physicstoday JOBS



# Inertial modes of a periodically forced buoyant drop attached to a capillary

Nicolas Abi Chebel,<sup>1,2,3</sup> Frédéric Risso,<sup>1,4</sup> and Olivier Masbernat<sup>1,3</sup>

<sup>1</sup>Fédération de recherche FERMAT, CNRS, Toulouse, France

<sup>2</sup>IFP—Energie Nouvelles, Rueil-Malmaison, France

<sup>3</sup>Laboratoire de Génie Chimique, CNRS & Université de Toulouse, France

<sup>4</sup>Institut de Mécanique des Fluides de Toulouse, CNRS & Université de Toulouse, France

(Received 1 February 2011; accepted 8 September 2011; published online 19 October 2011)

A drop of heptane attached to a capillary tip immersed in water is submitted to small amplitude volume oscillations. Its interface is imaged by means of a high-speed camera and its shape decomposed into spherical harmonics. The forcing frequency is varied over a large range including the frequencies of resonance of the three first modes of inertial shape oscillations. For a small drop, which remains almost spherical at rest, the geometrical constraint imposed by the attachment on the capillary tip causes the oscillation modes to be very different from those of a free drop. Surprisingly, the resonance of large drops is observed at the frequency predicted for a free, pure, and neutrally buoyant drop and mainly involves a single spherical harmonic; only the damping rate is observed to be moderately larger. Since it gives rise to oscillations close to this ideal case, the present experimental method could be used, complementary to quasi-static oscillation of a pendant drop, to investigate dynamic interfacial tension at high frequency of various fluid systems. © 2011 American Institute of Physics. [doi:10.1063/1.3646930]

## I. INTRODUCTION

Oscillation dynamics of drops and bubbles has been a subject of great interest due to the numerous applications it is involved in. In particular, it plays a major role in the deformation and break-up of bubbles and drops in turbulent flows, as shown by Risso and Fabre<sup>1</sup> and Galinat *et al.*<sup>2</sup> When the external forcing is unsteady, a balance between average turbulence intensity and interfacial tension is, in general, not sufficient for predicting break-up occurrence. When released in a turbulent flow, a drop indeed behaves as an oscillator and responds to the velocity fluctuations that have the same frequency, leading to resonance. Break-up, therefore, occurs either when individual eddies are strong enough or when the drop damping time is larger than the time between two significant fluctuations. A dynamic model accounting for this was established, the drop being described by a linear oscillator which is forced by a Weber number based on the instantaneous velocity fluctuation. This model is able to predict drop deformation and break-up statistics provided the eigenmodes of the drop shape are known. The determination of drop eigenfrequencies and damping rates is therefore essential for building predictive models of break-up in unsteady flows. However, these parameters are not known in many situations, especially when surfactants are present and modify the interfacial rheology. The purpose of the present work is to propose a reliable experimental method that allows the determination of the dynamics of the interface for any fluid system.

Let us start with some recalls about interface dynamics. Using linear theory, Rayleigh<sup>3</sup> was the first to calculate the vibration eigenmodes of an inviscid drop in vacuum in the absence of gravity. The theory developed by Rayleigh was generalized by Lamb<sup>4</sup> to the case of a bubble or a drop in a liquid medium. The method consists in writing the equations of motion inside and outside the particle, using the potential

flow theory. Assuming weak amplitude oscillations, the matching conditions at the interface are written for a sphere corresponding to the non-deformed drop. The calculation leads to a series of eigenmodes characterized by two integers  $(n, m)$ , a polar wavenumber  $n \geq 2$  and an azimuthal wavenumber  $m$  such as  $-n \leq m \leq n$ . To each eigenmode corresponds an eigenvector, the spherical harmonic  $Y_{n,m}$ , and thus a specific shape. The local position of the interface is given, in spherical coordinates by,

$$r = a(1 + A_{n,m}Y_{n,m}(\theta, \phi)\cos(\omega_n^*t)), \quad (1)$$

where  $a$  is the radius of the non-deformed drop and  $A_{n,m}$  the amplitude of the mode  $(n, m)$ . The corresponding eigenfrequency in the liquid-liquid case is given by

$$\omega_n^* = \sqrt{\frac{(n-1)n(n+1)(n+2)\sigma}{(\rho_d(n+1) + \rho_c)n a^3}}, \quad (2)$$

where  $\sigma$  is the interfacial tension,  $\rho_c$  and  $\rho_d$  are the densities of external and drop phases, respectively. One can notice that the eigenfrequency does not depend on  $m$ . Yet for a given value of  $n$ , there are  $2n+1$  values of  $m$ . The corresponding modes are degenerate and the non-axisymmetric modes ( $m \neq 0$ ) have the same frequency  $\omega_n^*$  as the axisymmetric mode ( $m=0$ ). The eigenmode calculations by Rayleigh and Lamb are set for inviscid fluids. For liquids of moderate viscosity and when there is no external forcing, the oscillation amplitude decays as  $\exp(-\beta_n t)$  where  $\beta_n$  is the damping rate corresponding to mode  $(n, m)$ . Lamb<sup>4</sup> calculated the damping rate for a drop in vacuum using the viscous potential flow theory. However, since the potential approach does not take into account the continuity of tangential stresses at the interface, it cannot be relied on to determine the damping rate for a drop in an immiscible liquid.

Miller and Scriven<sup>5</sup> considered a system with viscous fluids and calculated the linearized Navier-Stokes equations inside and outside the interface. At high Reynolds number, boundary layers develop in order to match the tangential velocities on both sides of the interface. Asymptotic expressions were obtained for the eigenfrequencies and the damping rates. They are written as a sum of two terms: the first accounts for the potential flow far from the interface and the other, proportional to the square root of the oscillation Reynolds number, accounts for the boundary layer flow. This work was extended by Prosperetti, who recognized the presence of a continuous spectrum<sup>6</sup> and examined the case of transient oscillations.<sup>7</sup> Marston,<sup>8</sup> then Lu and Apfel<sup>9</sup> obtained similar expressions to those of Miller and Scriven<sup>5</sup> and introduced, in the expression of the damping rate, a second order term that was omitted by Miller and Scriven.<sup>5</sup> As for the Rayleigh-Lamb theory, eigenmode  $(n, m)$  is represented by a spherical harmonic  $Y_{n,m}$ . The corresponding eigenfrequency and the damping rate are, respectively, given by,

$$\omega_n^{th} = \omega_n^* - \frac{\mu_d}{\rho_d a^2} F \sqrt{Re_{d,n}}, \quad (3)$$

$$\beta_n^{th} = \frac{\mu_d}{\rho_d a^2} [-2F^2 + G + F \sqrt{Re_{d,n}}], \quad (4)$$

with

$$F = \frac{(2n+1)^2 (\hat{\rho} \hat{\mu})^{\frac{1}{2}}}{2\sqrt{2} [n\hat{\rho} + n + 1] [1 + (\hat{\rho} \hat{\mu})^{\frac{1}{2}}]}, \quad (5)$$

and

$$G = \frac{(2n+1)[2(n^2-1) + (n+2)\hat{\mu} - (n-1)\hat{\rho}\hat{\mu} + 2n(n+2)\hat{\rho}\hat{\mu}^2]}{2[n\hat{\rho} + n + 1] [1 + (\hat{\rho} \hat{\mu})^{\frac{1}{2}}]}, \quad (6)$$

where  $\mu_c$  and  $\mu_d$  are, respectively, the viscosities of external and drop phases,  $\omega_n^*$  the Lamb frequency (Eq. (2)),  $\hat{\rho} = \rho_c/\rho_d$ , and  $\hat{\mu} = \mu_c/\mu_d$ .  $Re_{d,n}$  is the oscillation Reynolds number, based on dispersed phase density and viscosity,

$$Re_{d,n} = \frac{\rho_d a^2 \omega_n^*}{\mu_d}. \quad (7)$$

Expressions of  $\omega_n^{th}$  and  $\beta_n^{th}$  reduce to the potential expressions when one of the two phases is void.

Several works extended the theory to the case of an attached drop. (For a complete review, see Ref. 10 and references therein.) Strani and Sabetta considered a drop in contact with a portion of a sphere for either inviscid<sup>11</sup> or viscous<sup>12</sup> fluids. More recently, Bostwick and Steen<sup>10</sup> considered the case of a drop that is pinned on a circular contact line. In both cases, gravity was set to zero and the origin of coordinates was fixed with respect to the solid, so the decomposition into spherical harmonics was different from that used for a free drop. Each mode of oscillation then involved an infinite series of  $Y_{n,0}$  starting from  $n = 1$  and combining in a complex manner translation and deformation. The comparison with the case of the free drop is not straightforward,

particularly in a regime dominated by the harmonics  $Y_{1,0}$ . On the other hand, buoyancy was considered by Basaran and DePaoli<sup>13</sup> who numerically investigated the case of a drop hanging from a solid rod. These studies clearly demonstrate that drop attachment and buoyancy may drastically modify the proper modes of free oscillations.

The experimental verification of drop oscillation theory is challenging for a number of reasons. First, it is not convenient to study the oscillations of an actually free drop, i.e., not maintained by either a solid support or an additional force. Second, the drop shape has to be perturbed either by an initial disturbance or by a periodic forcing that must not change the nature of the physical mechanisms. Third, one ideally needs to accurately characterize the instantaneous shape of the drop at a rate that is much faster than the period of oscillation, which is typically tens to thousands hertz for drop diameters between 0.1 and 5 mm. Fourth, the presence of surface contaminants may also influence the results.

The first significant experimental contribution to this problem is due to Marston and Apfel<sup>14</sup> who developed a method, where a hydrocarbon drop is levitated in water by acoustic radiation. A modulation of the acoustic pressure is used to drive the shape oscillations, which are monitored by an interferometric technique. The measured resonance frequency of mode 2 for diameters ranging between 0.3 and 2 mm found a relatively good agreement with the prediction of inviscid linear theory (Eq. (2)). The same acoustic method was used by Trinh *et al.*<sup>15</sup> who investigated both forced and freely decaying oscillations of various organic compound drops in aqueous solutions. Measured resonance frequencies of modes 2, 3, and 4 showed a good agreement with the linear theory. Damping rate was determined for mode 2 and its value was about 20% larger than that predicted (Eq. (4)). Lu and Apfel<sup>16</sup> also performed acoustic levitation experiments of drops of hexane in water. Eigenfrequency of mode 2 well agreed with the theory while the measured damping rates were found 10% higher than the theoretical values. In these works, interface contamination was suspected to have a significant influence on the damping rate.

Several investigations of drop oscillations in contact with a solid surface have been carried out.<sup>17–20</sup> In all cases, the drop axial oscillations were imposed by periodical forcing. As predicted by Strani and Sabetta,<sup>12</sup> it turned out that the attachment constraint gives birth to a mode of lower frequency involving spherical harmonics  $n = 1$ . However, the exact interface dynamics depended on the way the drop was attached to the support and the oscillatory modes were found to be very different from those of a free drop.

The present work proposes an experimental method that allows a characterization of the drop dynamics based on a complete description of the interface in terms of spherical harmonics. It consists in studying the response to forced oscillations of a pendant drop attached to a capillary tube. The choice of this configuration was motivated by a number of considerations. First, it does not constrain fluid properties. Drop attachment eases a detailed analysis of the drop shape by means of video imaging, independently of drop volume or density difference. Then forced oscillations enable investigation of large viscosity fluids, in contrast with the case of

free oscillations decay for which the response to an initial disturbance would be too rapid. In addition, application of forced oscillations also allows studying the steady dynamic response of the drop shape at long times, avoiding the influence of initial transient stage. However, the use of common high speed imaging operating at a few thousand frames per second enables analysis of oscillation modes the frequency of which does not exceed a few hundred hertz, limiting the study to millimeter-range drop diameters. Another important point is the nature of the forcing that must not alter the interface dynamics. In the present study, the drop was submitted to small sinusoidal volume variations through the capillary by using a piezoelectric membrane. The first question arising from such a method is to determine whether or not small volume variations of an incompressible fluid drop can produce significant shape oscillations. Then, it is necessary to ensure that the linear domain could be accurately investigated while the drop keeps attached at the capillary tip. Furthermore, to be useful as a benchmark method that enables the comparison of different fluid systems, the drop dynamics must not be too complex, i.e., depending on too many parameters. The ideal method would induce the same response as that of a free drop in the absence of gravity, for which the theory is well-known in the absence of surfactant. Here, the attachment of the drop and the buoyancy force are likely to complicate the interface dynamics. In this paper, the case of a heptane drop immersed in water has been considered. Since the drop diameter is a few millimeters and the density difference is not small, buoyancy plays a significant role on the drop shape at rest. In what follows, we present a comprehensive investigation of the interface dynamics in this particular case. Comparing the results with the ideal case of a free and neutrally buoyant drop, the validity of the available theory is examined and the present method is evaluated as a potential tool for the characterization of the interface dynamics of more complex fluid systems.

## II. EXPERIMENTAL TECHNIQUE

### A. Experimental setup

A schematic representation of the experimental setup is given in Fig. 1. A dynamic tensiometer is used as a volume oscillation generator on a pendant drop (DSA 100 from Krüss). The external liquid phase is stored in a parallelepipedic optical-grade glass cell. A U-shaped stainless steel capillary tube of internal diameter 1.2 mm is immersed in the external phase and connected to a syringe allowing the drop production at the capillary tip. The internal phase is stored in a cell mounted between the capillary and the feeding syringe (2). One of the cell walls (2'') is a piezoelectric membrane, which can be driven by a periodic motion of variable frequency and amplitude. The motion of the membrane leads to periodic variation of the cell volume and, thus, of the attached drop volume. Images of the oscillating drops are captured by a high speed camera (Photron APX). The image size is  $1024 \times 1024$  pixel and the field size has been set to  $7 \times 7 \text{ mm}^2$ , leading to a spatial resolution close to  $7 \text{ } \mu\text{m}/\text{px}$ . With this image format, the grabbing rate can be varied from 60 to 2000 fps, depending on the oscillation frequency. A  $10 \text{ cm} \times 10 \text{ cm}$  surface LED backlight is used as light source.

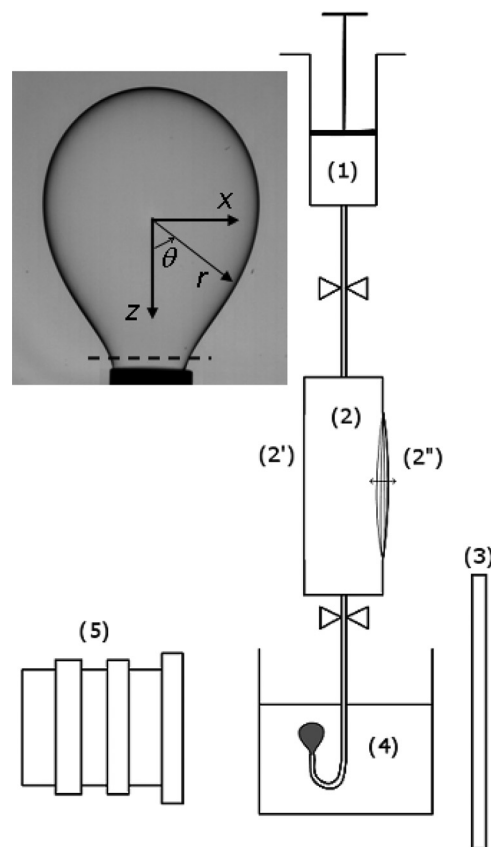


FIG. 1. Experimental setup: (1) feeding syringe, (2) drop phase cell, (2'') glass window, (2'') piezoelectric membrane, (3) LED backlight, (4) external phase, and (5) high-speed camera. The horizontal dashed line on the photograph delimits the region taken into account for the determination of the drop volume.

### B. Phase system

Distilled water was used as the external phase while the drop phase is composed of n-heptane (p.a. grade), used as purchased without further purification. The interfacial tension of the pure heptane/water system at  $25 \text{ } ^\circ\text{C}$  has been reported<sup>21</sup> to be  $51 \text{ mN}\cdot\text{m}^{-1}$ . Interfacial tension of the present system was measured by the pendant drop method. The interfacial tension was observed to slightly decrease with time over a period of 20 min, indicating the presence of surface active contaminants. Working with a non-ultra-pure system is a deliberate choice in this study. First, the interface rheology of such a system is solely governed by the interfacial tension at equilibrium and there is no measurable viscoelastic modulus in the quasi-static deformation regime (i.e., in the limit of low frequency pulsation). Therefore, it is considered here as a reference case, to be later compared to more complex interfacial rheology systems such as those encountered in crude oil-water emulsions.<sup>23</sup> Then, as it is a tedious task to work with pure liquid phases through the whole equipment, choice was made to first start with a non-ultra-pure system and *a posteriori* to evaluate the sensitivity of oscillation modes parameters (frequency and damping rate) to the presence of contaminants at the interface. During an experiment under oscillations, the interface age varied between 1 and 10 min, which corresponds to an interfacial tension ranging between 48 and  $46.5 \text{ mN}\cdot\text{m}^{-1}$ . An intermediate value of  $47 \text{ mN}\cdot\text{m}^{-1}$  has



TABLE I. Fluid properties at 25 °C.

	Water	n-Heptane
Density $\rho$ (kg · m <sup>-3</sup> )	997	680
Viscosity $\mu$ (Pa · s)	$0.9 \cdot 10^{-3}$	$0.4 \cdot 10^{-3}$
Interfacial tension $\sigma$ (N · m <sup>-1</sup> )	$47 \cdot 10^{-3}$	

been chosen as the nominal interfacial tension for the present experiments. Other properties of the fluids are reported in Table I at 25 °C, which was the ambient temperature of present experiments.

### C. Operating parameters and experimental procedure

For a given liquid-liquid system, the operating parameters are the drop volume or diameter, the forced oscillation frequency and amplitude, and the capillary diameter. The diameter range of the drops is imposed by the time resolution of the camera. From Eq. (3), the frequency of mode  $n$  of a nonconstrained drop is close to  $\omega_n^*$  (Eq. (2)) which is a power law decaying function of the drop diameter  $d$  and a growing function of mode index  $n$ . In order to correctly analyze the shape oscillations of mode  $n$ , the mode frequency must be significantly lower than the maximum grabbing frequency of the camera, which is 2 kHz. The minimum diameter for which mode 5 can be determined with reasonable accuracy must verify

$$\omega_5^*/2\pi = f_{aq}/10 = 200 \text{ Hz.} \quad (8)$$

From Eq. (2), this condition corresponds to a minimum drop diameter  $d_{min} \approx 3$  mm. This value is close to the capillary length of the n-heptane/water system given by,

$$\lambda_c = \sqrt{\frac{\sigma}{\Delta\rho g}} = 3.9 \text{ mm.} \quad (9)$$

As a consequence, the drop range for which the four first shape oscillation modes can be accurately analyzed corresponds to a range of Bond number,  $Bo = (a/\lambda_c)^2$ , for which the pendant drop shape at rest significantly deviates from spherical shape. The maximum drop diameter  $d_{max}$  corresponds to the drop detachment that can be evaluated from the force balance between buoyancy and surface tension forces, leading to

$$d_{max}^3 = 6\lambda_c^2 d_c, \quad (10)$$

where  $d_c$  is the capillary tube internal diameter. Equation (10) shows that the capillary diameter determines the maximum drop diameter for a given set of fluids and therefore the width of the drop diameter range in the present experiments. As it must be chosen significantly smaller than the drop diameter, setting  $d_c < d_{max}/4$  leads to the following framing:

$$\frac{d_{min}^3}{6\lambda_c^2} = 0.3 \text{ mm} < d_c < \sqrt{\frac{3}{32}}\lambda_c = 1.2 \text{ mm.} \quad (11)$$

The capillary diameter was set to its maximum value,  $d_c = 1.2$  mm, in order to maximize the investigated drop diameter range.

TABLE II. Drop diameter, Bond, and Reynolds numbers.

Drop diameter $d = 2a$ (mm)	3.6±0.2	4.19±0.02	4.48±0.02
$Bo = \frac{\Delta\rho g a^2}{\sigma}$	0.22	0.29	0.33
$Re_{d,2} = \frac{\rho_d a^2 \omega_2}{\mu_d}$	1255	1345	1390

Three drop diameters have been considered in this study: 3.6 mm, 4.19 mm, and 4.48 mm. Corresponding Bond numbers and oscillation Reynolds numbers are reported in Table II. Note that the Bond number ranges outside the spherical domain, so the drop diameter is defined by that of an equivalent sphere of same volume. The volume considered here is calculated from spatial integration of the region delimited by the drop contour and a horizontal line arbitrarily set at  $\sim 0.2$  mm above the capillary tip. Prior to each measurement series, the glass cell, the disperse phase cell, and the capillary were successively cleaned with toluene, heptane, ethanol, and distilled water. A heptane drop is produced at the capillary tip immersed in water. The attached drop is submitted to periodic low amplitude volume variation at a frequency ranging between 0.1 and 150 Hz. The volume amplitude is chosen in order to maximize the amplitude of the drop shape response at the current forcing frequency while keeping the response in the linear domain, which will be defined precisely in Sec. III C. For the drop diameter range considered, the maximum relative volume variation is 3.5%.

### D. First observations

Sequences of images of a 4.19 mm diameter drop oscillating at different frequencies are presented in Fig. 2. At given frequencies, resonance phenomena take place and amplified surface waves are clearly observed. In this figure, selected frequencies are 1 Hz, 29 Hz, 50 Hz, and 77 Hz (ranging from row a to d, respectively). The last three values are close to the theoretical values  $\omega_2^{th}$ ,  $\omega_3^{th}$ , and  $\omega_4^{th}$  of a free oscillating heptane drop of same volume. Middle column (2) displays the mean shape while pictures of columns (1) and (3) correspond to the instants where drop deformation is at maximum. No shape oscillation is observed at 1 Hz (row a), inertial effects being not present at this low frequency. Images displayed in row b show elongated/flattened shapes typical of spherical harmonic  $Y_{2,0}$ . Likewise, drop shapes displayed in row c (50 Hz) and d (77 Hz) can be readily matched to the theoretical shapes of Rayleigh modes 3 and 4, respectively. These sequences clearly demonstrate, on the one hand, the excitation of shape oscillations from small volume amplitude variations and, on the other hand, the good matching of the resonance frequencies with theoretical values of free oscillating drops.

### E. Interface description from image processing

Since the drop remains axisymmetric during oscillations the use of a single view is sufficient to obtain a complete description of the drop interface. The five first periods of each video sequence are discarded in order to ensure that the oscillations have reached a steady state. Images are then

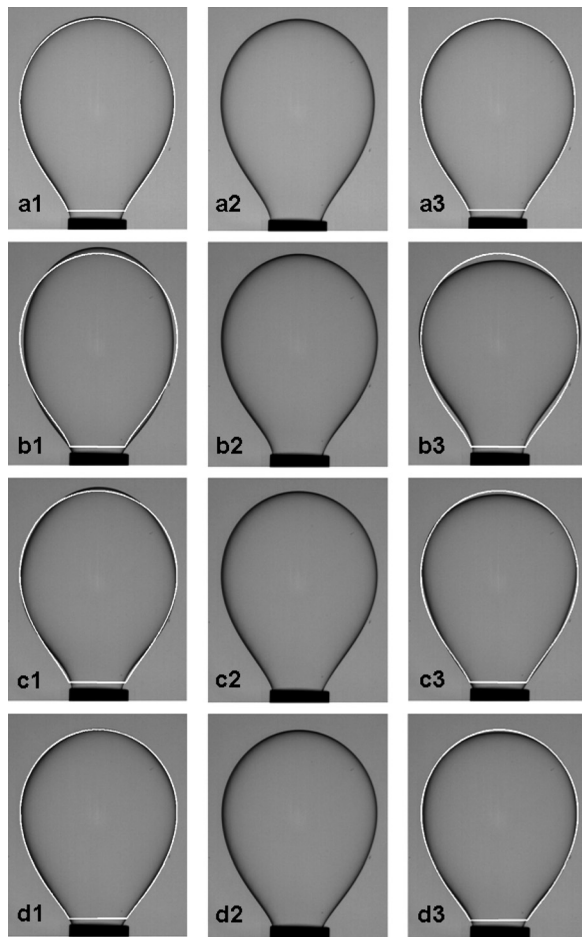


FIG. 2. Images of an oscillating drop of  $d=4.19$  mm. Forcing frequency: 1 Hz (ai), 29 Hz (bi), 50 Hz (ci), 77 Hz (di); Instants of maximum deformation ( $i=1$  and  $3$ ), mean shape ( $i=2$ ). White curves correspond to mean shape.

processed as follows. First, a rough detection of the drop is obtained by applying a simple threshold to the grey scale images derived from Otsu's method.<sup>22</sup> This operation provides the drop boundary location with an accuracy of 1 pixel. Then, for each external point of the interface a sub-pixel interpolation<sup>24</sup> is applied in three directions with neighboring pixels to determine the exact position matching the threshold value. From noise analysis of the local curvature of the detected contour, the final resolution can be estimated to 0.1 pixel, which is consistent with the scattering observed on the spherical harmonics time signals.

The local position of the interface, expressed in spherical co-ordinates, is first fitted by a  $r(\theta)$  polynomial of order 10. This polynomial is then written as a combination of spherical harmonics which reduce to Legendre polynomials  $P_n$  in the axisymmetric case for which  $m=0$ ,

$$r(t)/a = A_0(t) + \left( \sum_{n=2}^{10} A_n(t) Y_n(\theta) \right), \quad (12)$$

where  $a$  is the average radius of the equivalent spherical drop and  $A_n(t)$  is the instantaneous dimensionless amplitude of the spherical harmonic  $Y_n(\theta) = Y_{n,0}(\theta) = P_n(\cos(\theta))$ .  $A_0(t)$  is related to the volume variation of the drop and

describes the forcing. The origin  $z_c$  of the spherical co-ordinates has been chosen such as  $A_1=0$  at each instant. Based on this definition, amplitudes  $A_n(t)$  for  $n \geq 2$  only represent drop deformation while the translation is given by  $z_c(t)$ . The decomposition into spherical harmonics being the same, comparisons of the present results with the theory developed for a free drop will thus be straightforward. On the other hand, it is worth mentioning that the decomposition used by Strani and Sabetta<sup>11,12</sup> and Bostwick and Steen,<sup>10</sup> who studied neutrally buoyant pinned drop, was fixed and thus led to a different decomposition with  $A_1 \neq 0$ .

The expression of the instantaneous drop shape can then be written as the sum of two terms,

$$r(t)/a = \left( \overline{A_0} + \sum_{n=2}^{10} \overline{A_n} Y_n(\theta) \right) + \left( \Delta A_0(t) + \sum_{n=2}^{10} \Delta A_n(t) Y_n(\theta) \right), \quad (13)$$

where the overbar denotes time averaging. The first term corresponds to the average shape of the oscillating drop, which is the shape of the drop at rest. Since the drop is attached and submitted to gravity, its shape at rest is not spherical and can be described by a linear combination of spherical harmonics. The second term is related to the shape oscillations and is a linear combination of spherical harmonics with time dependent coefficients  $\Delta A_n(t)$ .




As mentioned above, the measurement accuracy of  $r(t)$  is 0.1 pixel, which corresponds to  $7 \cdot 10^{-4}$  mm and represents less than 0.15% of the radius of the present drops. This estimation is confirmed by the examination of the time evolution of the drop equivalent radius, where the noise level is about  $10^{-4}$  mm. An additional error in the determination of  $\Delta A_n(t)$  might be introduced by the polynomial fitting but it was checked that, with a polynomial of order 10, the noise level remained below  $10^{-4}$  mm. However, it turned out that measurement errors are not the main source of uncertainty in the determination of the amplitudes  $\Delta A_n(t)$ . In fact, each drop is manually generated with the feeding syringe and its size manually controlled with the help of two cursors on the live image. For a given series of experiments on the same drop volume, the drop is renewed several times (drop residence time never exceeded 10 min) and the relative accuracy on the average drop volume is about 5%. Such a volume difference corresponds to a variation of 7% of the natural frequency of the oscillating modes and consequently shifts the resonance curves. The evaluation of the amplitude uncertainty resulting to initial volume difference is discussed in Sec. III C.

### III. RESULTS AND DISCUSSION

#### A. Mean shape

Table III shows pictures of the drop shape at rest (or the mean shape during oscillation) as well as its spectral decomposition into spherical harmonics for the three investigated drop sizes. Due to buoyancy and the attachment to the capillary, a significant departure from sphericity is observed,

TABLE III. Spectral decomposition of the mean drop shape into spherical harmonics for the three drop diameters. (Departures from sphericity are due to buoyancy.)

Diameter $2a$ (mm)	3.60	4.19	4.48
Image			
$\bar{A}_2$	0.0906	0.1449	0.1653
$\bar{A}_3$	0.0416	0.0748	0.0878
$\bar{A}_4$	0.0273	0.0580	0.0708
$\bar{A}_5$	0.0176	0.0431	0.0555

leading to a series of finite amplitudes  $\bar{A}_n$ , starting by a maximum value for  $n=2$ , and then decreasing as  $n$  is increased. The predominance of spherical harmonic  $Y_2$  results from the elongated shape of the drops, while  $Y_3$  originates from the dissymmetry with respect to the equatorial plane (one pole is free and another is attached). For a given harmonic, the two largest drops ( $d=4.19$ , and  $4.48$  mm) exhibit much higher amplitudes than the smaller one ( $d=3.6$  mm). This larger deformation is related to the existence of a connecting neck between the drop and the capillary tip, which is clearly visible for the two largest drops whereas it is absent for the smallest one.

## B. Time evolution

Drop shape analysis is performed for each captured image at current time  $t$ . Time evolution of the drop volume variation  $\Delta V$ , the center location  $z_c$ , and the amplitude  $A_n$  of the first 11 spherical harmonics ( $n=0$  to 10) have been determined. The forcing signal,  $\Delta V$ , normalized by the mean drop volume  $\bar{V}$  as well as the time evolution of the normalized drop centre location,  $z_c/a$ , are shown in Fig. 3 while the oscillating parts of the spherical harmonics amplitudes  $\Delta A_0$ ,  $\Delta A_2$ ,  $\Delta A_3$ , and  $\Delta A_4$  are displayed in Fig. 4. This example

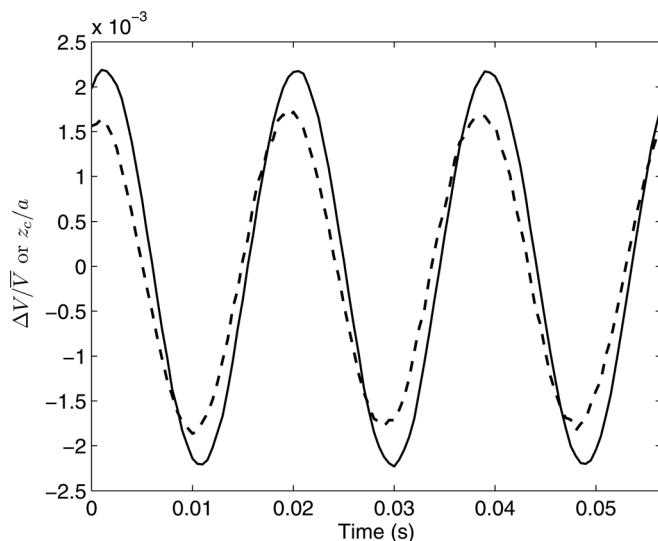


FIG. 3. Time evolution of the non-dimensionalized drop volume  $\Delta V/\bar{V}$  (solid line) and of the non-dimensionalized drop center position  $z_c/a$  for  $d=4.48$  mm (dashed line) at a forcing frequency of 52.6 Hz.

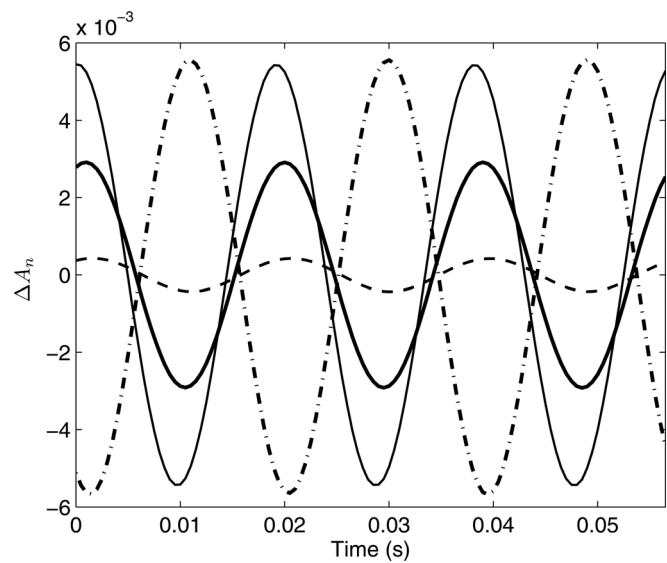


FIG. 4. Time evolution of the spherical harmonics for  $d=4.48$  mm. ---  $\Delta A_0$ , —  $\Delta A_2$ , —  $\Delta A_3$ , - -  $\Delta A_4$ . (The decomposition is done according to Eq. (13).)

corresponds to a 4.48 mm diameter drop and a forcing frequency equal to 52 Hz. All signals are almost perfectly sinusoidal and can therefore be described according to the following equations:

$$\Delta V(t) = \bar{V} \tilde{V} \cos(\omega t), \quad (14)$$

$$z_c(t) = a \tilde{z}_c \cos(\omega t + \varphi_z), \quad (15)$$

$$\Delta A_n(t) = \tilde{A}_n \cos(\omega t + \varphi_n). \quad (16)$$

All response signals have the same frequency  $\omega$  as the forcing signal, which is usually the case for a forced linear oscillator. Each response signal is then characterized by its amplitude and its phase shift with regard to  $\Delta V$ .

## C. Response to the forcing amplitude and linearity

The linearity of the drop response to a sinusoidal volume variation is examined by varying, at a given frequency, the forcing amplitude  $\Delta V$ . Forcing frequencies are selected near the resonance of each spherical harmonic and the resulting amplitudes  $\tilde{A}_n$  are analyzed. A typical result is illustrated in Fig. 5, where the amplitudes of the first four spherical harmonics ( $n=2$  to 5) have been plotted as a function of  $\tilde{V}$  for a 4.48 mm drop excited at 25 Hz, which corresponds to the resonance of mode 2. In the considered range of forcing amplitudes, each  $\tilde{A}_n$  is a linear function  $\tilde{V}$ . The slopes differ from one mode to the others, the largest one being observed for  $n=2$ .

For all tested cases, oscillations were proved to remain in the linear domain provided  $\tilde{V}$  was less than 3.5%. All measurements presented in the next sections have been obtained with a volume amplitude well below this limit.  $\tilde{A}_n$  can thus be normalized by  $\tilde{V}_n$ , allowing the amplitudes of the spherical harmonics to be compared independently of the forcing level. When carried out at the same frequency and for different forcing amplitudes, the normalization leads to

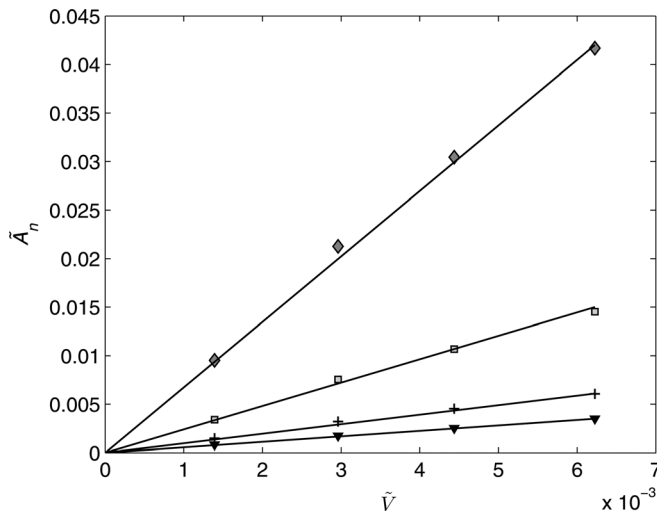


FIG. 5. Dimensionless amplitude  $\tilde{A}_n$  of the spherical harmonics as a function of the volume forcing amplitude  $\tilde{V}$  for  $d = 4.48$  mm at 25 Hz.  $\diamond$ :  $n = 2$ ,  $\square$ :  $n = 3$ ,  $\nabla$ :  $n = 4$ ,  $+$ :  $n = 5$ . (The decomposition is done according to Eq. (13).)

several equivalent measurement points. Therefore the scattering of the values of the  $\tilde{A}_n/\tilde{V}_n$  ratio for each experiment provides an evaluation of the accuracy of the experimental determination of the amplitude. The overall uncertainty on the amplitude  $\Delta(\tilde{A}_n/\tilde{V}_n)/(\tilde{A}_n/\tilde{V}_n)$  was found to be of the order of 5%.

For the present purpose of designing an experimental technique for the characterization of the interface dynamics, it is an important finding that linear shape oscillations can be generated by small volume oscillations. We may wonder how energy is transferred from volume variations to surface modes. Assuming that the kinetic energy of the liquid that is injected into the drop through the capillary is directly transferred to inertial shape oscillations would lead to the following scaling:

$$\tilde{A}_n \propto \rho_d (\omega \tilde{A}_0)^2 \propto \rho_d (\omega \tilde{V})^2, \quad (17)$$

which contradicts the linear dependence observed between  $\tilde{A}_n$  and  $\tilde{V}$ . The coupling between the volume and the drop shape rather results from geometrical considerations. First, since the drop at rest is not spherical ( $\tilde{A}_n \neq 0$ ), changing its volume necessarily changes the amplitude of the various spherical harmonics. Second, we must have in mind that the volume of a drop performing oscillations described by a single spherical harmonics  $Y_n$  with  $n \geq 2$  is not constant. Therefore, even if  $Y_n$  with  $n \geq 2$  are orthogonal to each others, any constraints imposed to the volume can generate a coupling between them. Natural coupling between volume and shape variations has indeed already been observed to play a role in other situations.<sup>25</sup> The exact understanding of the mechanism that transfers energy from volume to shape oscillation is beyond the scope of the present work. For the present purpose, the point is that shape oscillations are generated, the amplitudes of which are independent of the amplitude of the forcing when normalized by that of the volume variation. In the following, we will only consider amplitudes normalized by  $\tilde{V}$ .

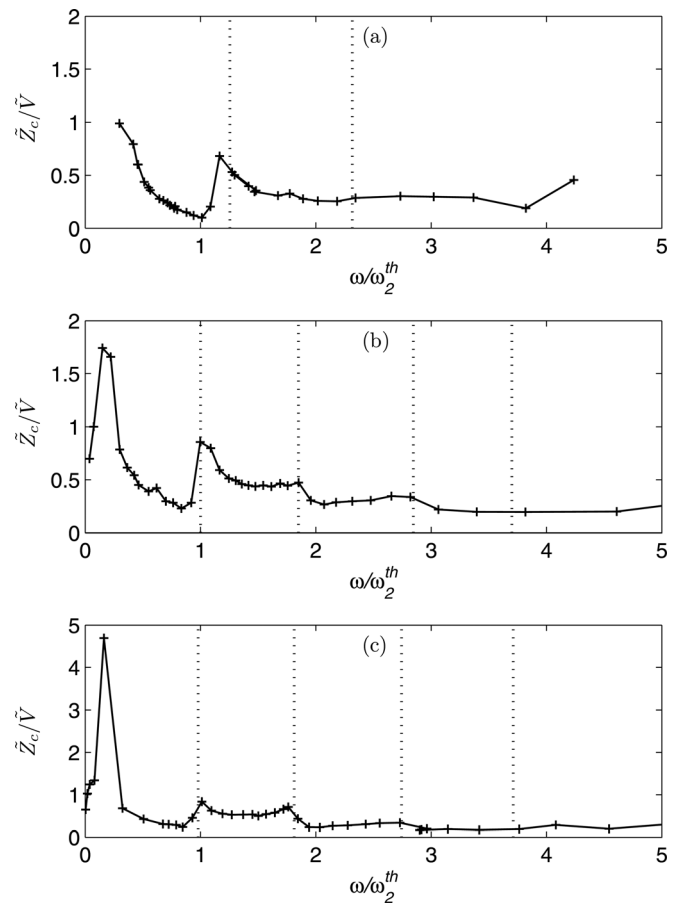


FIG. 6. Translation amplitude of the drop center  $\tilde{Z}_c/\tilde{V}$  as a function of the forcing frequency. (a)  $d = 3.6$  mm, (b)  $d = 4.19$  mm, (c)  $d = 4.48$  mm. Vertical dotted lines mark measured resonance frequencies of the shape modes.

#### D. Response to the forcing frequency

For each of the three studied drop diameters, the forcing frequency was swept from 1 to 150 Hz. Figure 6 shows the normalized amplitude  $\tilde{Z}_c/\tilde{V}$  of the drop center against the forcing frequency  $\omega$ , which has been normalized by theoretical frequency  $\omega_2^{th}$  of the second mode of a free drop. Figures 7–9 display the normalized amplitude  $\tilde{A}_n/\tilde{V}$  together with the corresponding phase shift  $\varphi_n$ .

Concerning  $\tilde{Z}_c/\tilde{V}$ , a peak of significant height is observed at low frequency around  $\omega_2^{th}/5$ . It corresponds to the resonance of a translation mode, which is due to the drop attachment to the capillary. When the drop volume increases, its centre moves away from the capillary tip mainly due to buoyancy while capillary forces tend to bring the drop back to its initial position. The resonance peak strongly increases with the drop size, suggesting that the larger drops have more freedom to perform translation, probably because of the existence of the liquid neck which attaches the drop to the capillary. A secondary peak is also visible at the resonant frequency of the first of the shape modes, denoted by vertical dotted lines in Fig. 6. At variance with the major peak, the height of the secondary peak of  $\tilde{Z}_c/\tilde{V}$  is almost independent of the drop diameter, just as is the height of the peaks observed in the response of the spherical harmonics (Figs. 7–9). Moreover, its height is an order of magnitude



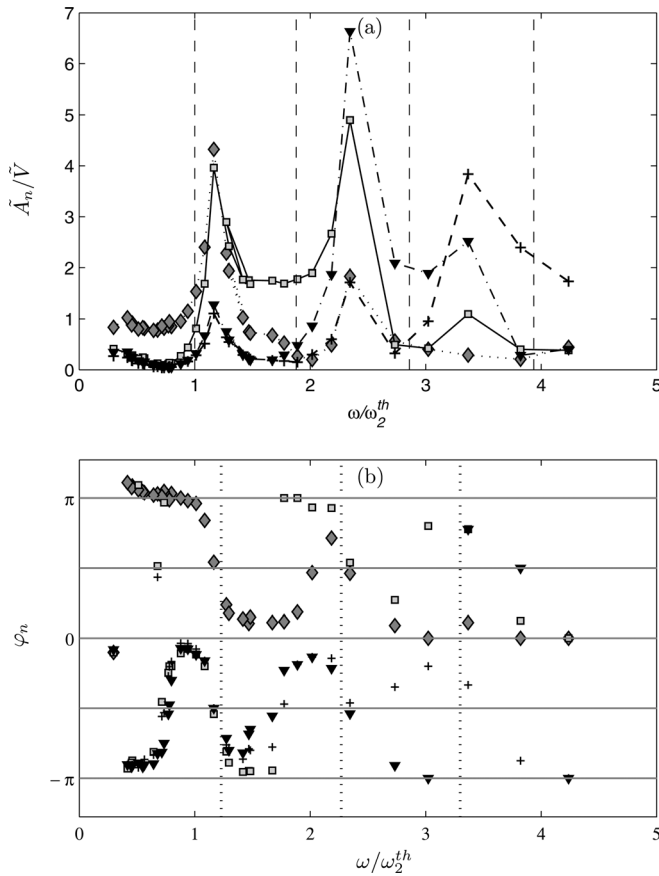


FIG. 7. (a) Amplitudes  $\tilde{A}_n/\tilde{V}$  of spherical harmonics and (b) phase shifts  $\varphi_n$  between spherical harmonic oscillations and volume forcing as a function of the forcing frequency for  $d=3.6$  mm.  $\diamond$ :  $n=2$ ,  $\square$ :  $n=3$ ,  $\nabla$ :  $n=4$ ,  $+$ :  $n=5$ . Vertical dotted lines mark measured resonance frequencies of the shape modes. Vertical dashed lines mark theoretical resonance frequencies predicted by Eq. (3).

smaller than those of the spherical harmonics. We shall therefore consider that the resonance of the shape modes is not significantly affected by the translation mode.

We consider now the response of the drop shape as a function of the forcing frequency. For each drop diameter, the plots of  $\tilde{A}_n/\tilde{V}_n$  displayed in Figs. 7–9 for  $2 \leq n \leq 5$  show several peaks, the amplitudes of which are listed in Tables VI, VII, and VIII of Appendix A. We start by analyzing the behavior of the two largest drop sizes ( $d=4.19$  and  $4.48$  mm); the more complex response of the smallest drop ( $d=3.6$  mm) will be discussed later. Each spherical harmonic  $Y_n$  exhibits a major peak at a frequency close to  $\omega_n^{th}$  and secondary peaks around  $\omega_p^{th}$  for  $p \neq n$ . Let us take, for example, the first resonance frequency,  $\omega = \omega_2^{th}$ . The drop interface is mainly defined by the spherical harmonic  $Y_2$  (dominant peak) with more or less significant contribution of the other spherical harmonics (secondary peaks). A similar behavior is observed for the three other resonance frequencies, which are respectively governed by the spherical harmonics  $Y_3$ ,  $Y_4$ , and  $Y_5$ . In other words, the drop shape is observed to enter into resonance each time  $\omega$  matches the eigenfrequency  $\omega_n^{th}$  of a mode of a free drop, the drop oscillation being dominated by the corresponding spherical harmonics  $Y_n$ .

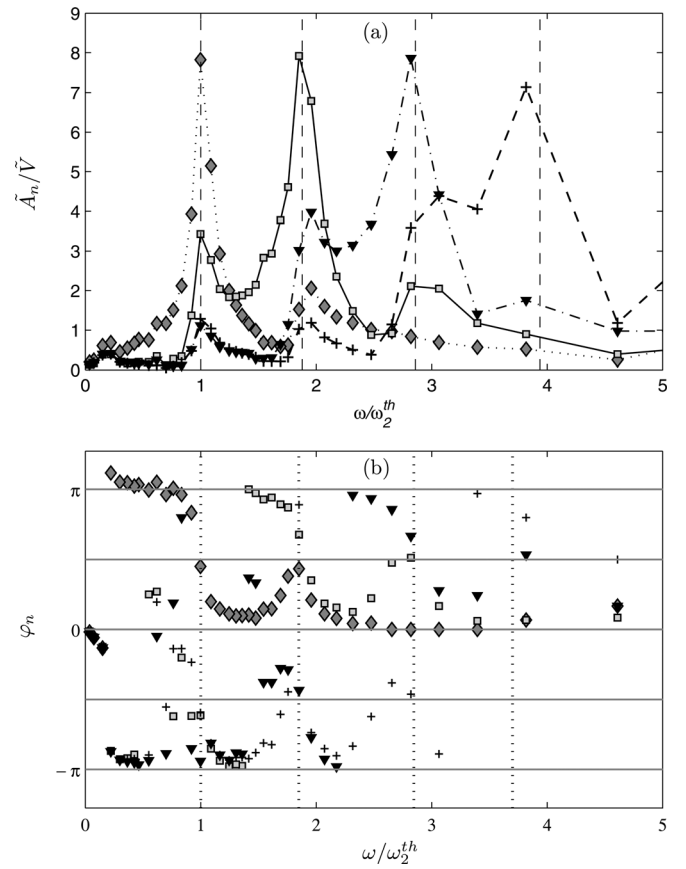


FIG. 8. (a) Amplitudes  $\tilde{A}_n/\tilde{V}$  of spherical harmonics and (b) phase shifts  $\varphi_n$  between spherical harmonic oscillations and volume forcing as a function of the forcing frequency for  $d=4.19$  mm.  $\diamond$ :  $n=2$ ,  $\square$ :  $n=3$ ,  $\nabla$ :  $n=4$ ,  $+$ :  $n=5$ . Vertical dotted lines mark measured resonance frequencies of the shape modes. Vertical dashed lines mark theoretical resonance frequencies predicted by Eq. (3).

Further insights into the resonance mechanism are obtained by considering phase shifts. For each investigated shape modes,  $\Delta A_n$  is observed to be in phase opposition with  $\Delta V$  ( $\varphi_n = \pi$ ) at low frequency, i.e., for  $\omega < \omega_n^{th}$  and far from the resonances of other modes. This indicates that the actual forcing signal is  $-\Delta V$ . For  $n=2$ , this means that a slow decrease—relative to the mode frequency—of the drop volume  $V$  induces the flattening of the drop shape ( $\Delta A_2 < 0$ ), while decreasing  $V$  causes the lengthening of the drop ( $\Delta A_2 > 0$ ). For any  $n$ ,  $\varphi_n$  evolves as if  $Y_n$  would fully characterize the drop shape oscillations at resonance: it decreases abruptly as the forcing frequency approaches the resonance frequency, where it equals the expected value  $\pi/2$ , and then decreases towards zero. Concurrently, around the resonance, the phases of the secondary spherical harmonics are either in phase or in phase opposition with that of the principal one.

Altogether, these results suggest that the dynamics of the two largest drops is not very different from that of a free drop in the absence of gravity, showing a resonance close to  $\omega_n^{th}$  with a shape dominated by  $Y_n$ . However, as well as for the shape at rest, the role of the secondary harmonics is to adapt the drop deformation to the constraint imposed by the attachment to the capillary. This is well illustrated in Fig. 2. As an example,  $Y_2$  is symmetric with regard to the drop

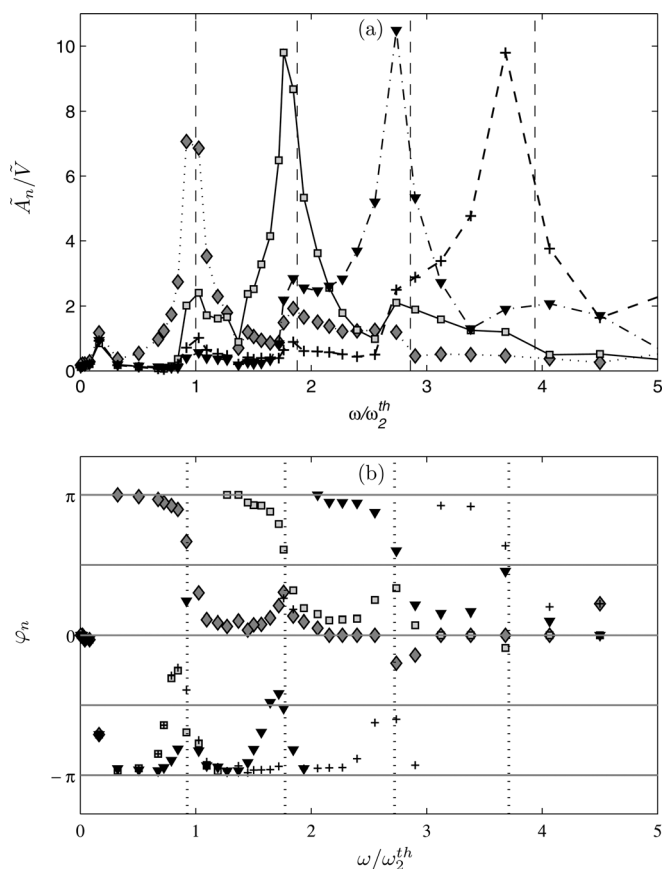


FIG. 9. (a) Amplitudes  $\tilde{A}_n/\tilde{V}$  of spherical harmonics and (b) phase shifts  $\varphi_n$  between spherical harmonic oscillations and volume forcing as a function of the forcing frequency for  $d=4.48$  mm.  $\diamond$ :  $n=2$ ,  $\square$ :  $n=3$ ,  $\nabla$ :  $n=4$ ,  $+$ :  $n=5$ . Vertical dotted lines mark measured resonance frequencies of the shape modes. Vertical dashed lines mark theoretical resonance frequencies predicted by Eq. (3).

equator, which cannot be the case for an attached drop submitted to mode-2 oscillations, especially in its flattening stage when  $\varphi_2 = \pi$  (Fig. 2(b3)). The contribution of harmonics of odd order, in particular  $Y_3$ , has thus to be accounted for in mathematical description of the shape. Also, when submitted to mode-3 oscillations, due to the attachment at the bottom, the drop shape at  $\varphi_3 = 0$  (Fig. 2(c3)) cannot be the reverse pattern of that corresponding to  $\varphi_3 = \pi$  (Fig. 2(c1)), resulting in a significant contribution of  $Y_4$ . Similarly, a contribution of  $Y_5$  on mode-4 oscillations can be deduced from Fig. 2(d3). Note that the relative contribution of the secondary spherical harmonics at resonance is reduced for the 4.48 mm drop (Fig. 9) compared to the 4.19 mm drop (Fig. 8). This suggests that the largest attached eigenmodes are closer to those of a free drop, underlining an effect of drop size on shape oscillations.

The shape dynamics of the smallest drop ( $d=3.6$  mm) are both qualitatively and quantitatively different (Fig. 7). The first resonance peak, the frequency of which is equal to  $1.15 \omega_2^{th}$  or  $0.61 \omega_3^{th}$ , involves mainly spherical harmonics  $Y_2$  and  $Y_3$  with similar amplitudes, while the contributions of  $Y_4$  and  $Y_5$  are small. The second resonance has a frequency equal to  $1.25 \omega_3^{th}$  or  $0.82 \omega_4^{th}$  and is dominated by  $Y_{3,0}$  and  $Y_{4,0}$  with comparable amplitudes. The third one involves similarly  $Y_4$  and  $Y_5$  and has a frequency in between  $\omega_4^{th}$  and

$\omega_5^{th}$ . (Note that a fourth resonant peak is not detected in the investigated frequency range because eigenfrequencies increase as the drop size decreases.) Moreover, the phases of the oscillations all match  $\pm\pi/2$  at resonance. Therefore, although it is much more spherical than the two largest ones, the dynamics of the smallest drop turn out to be very different from that of a free drop.

A number of theoretical<sup>10–13</sup> or experimental<sup>17–19</sup> works have studied oscillations of constrained drops. However, due to buoyancy, the way the drop is connected to the support, or the viscosity and density ratios, none of the considered situations is similar to the present one. The two closest situations are those addressed by Strani and Sabetta<sup>11,12</sup> and Bostwick and Steen.<sup>10</sup> The different basis used to decompose the drop shape does not allow a direct quantitative comparison of the mode amplitudes with our results. However, resonant frequencies are not affected by this decomposition. Strani and Sabetta<sup>11</sup> determined theoretically the proper modes of oscillations of a drop which is attached to a spherical bowl for the inviscid and neutrally buoyant case. In particular, they showed that the frequency  $\omega/\omega_n^*$  of all attached modes increases as the size of the bowl increases. Assimilating our capillary tube-to-drop diameter ratio ( $d_c/d$ ) to their bowl size-to-drop diameter, one can compute their attachment angle  $\alpha$ , which is 15.5, 16.6, and 19.5° for 4.48, 4.19, and 3.36 mm drop diameters, respectively. In this range, Fig. 3 of Strani and Sabetta<sup>11</sup> shows that the relative increase of  $\omega_n$  for all the three drops at all modes is very small. Hence,  $\omega_n$  values are very close to the theoretical values of the free oscillating drop. This trend could be consistent with our two larger drops, where the relative variation of  $\omega_n$  is smaller than 3% for modes 2, 3, and 4, but not with the smaller one, where the relative variation is 15%, 35%, and 16% for modes 2, 3, and 4, respectively.

Bostwick and Steen<sup>10</sup> also addressed the case of an inviscid neutrally buoyant drop but with a different attachment constraint, consisting in pinning the drop on a circle instead of a bowl as in Strani and Sabetta.<sup>11</sup> Both theories agree when the pinned region reduces to a single point but strongly differ in the vicinity of this limit. The only case which is fully documented by Bostwick and Steen<sup>10</sup> concerns the case of a drop in vacuum. For this case, their Fig. 2 shows that the frequency evolves in a very complex manner with the size of the attachment region. Taking the diameter of our capillary as that of their pinning circle, their attachment parameter  $a$  equals, respectively, 0.942, 0.958, and 0.964 for  $d=3.6$  mm,  $d=4.19$  mm, and  $d=4.48$  mm. In this range, in contrast with Strani and Sabetta,<sup>11</sup> mode frequencies steeply increase as  $a$  is decreasing from unity, which corresponds to a single point of attachment. This would not be in contradiction with our results provided that the largest drops ( $a=0.958$  and  $0.964$ ) would be assimilated to the limit case  $a=1$  while the smaller one ( $a=0.942$ ) would not. However, the experimental peak amplitude of the translation mode (Fig. 6) is observed to increase as the drop size is increasing, in contradiction with what is expected from the theoretical prediction. Note also that the decomposition of the attached modes into Legendre polynomials for our largest drop ( $a=0.964$ , Table VI) noticeably differs from the

theoretical decomposition at  $a = -0.99$  reported in Appendix B of Bostwick and Steen.<sup>10</sup> Despite a different modal decomposition, we think that this difference is significant because the amplitude of the translation is negligible compared to that of mode 2 for our largest drop.

The difference between the two theories demonstrated that the way the drop is attached may greatly alter the shape modes, despite the existence of the mode that couples translation to deformation in both cases. The major discrepancies between our experiments and these theories are therefore not surprising when considering gravity effect. The point is that increasing the size modifies the equilibrium shape of the drop close to the capillary (see Table III) which radically changes the attachment constraint.

Unexpectedly, we can thus conclude that the larger is the drop, the more the interface dynamics gets closer to that of a free neutrally buoyant drop. The deviation from sphericity of the average drop shape induced by buoyancy has indeed a weak influence on the drop shape oscillations. On the other hand, by causing the development of a fluid neck which smoothly connects the drop to the capillary, buoyancy relaxes the coupling between the various shape oscillation modes. If the present experiments demonstrate the existence of this particularly interesting regime, they are not sufficient to determine its domain in the Bond number- $d_c/d$  plane. It is probable, however, that this regime is restricted to rather large drop volumes that are close to the limit of detachment from the capillary. In the Sec. III E, the shape modes of the two largest drops are analyzed in detail.

### E. Eigenmodes of the largest attached drops

The eigenvector  $\mathbf{V}_n$  of the proper modes of the two largest attached drops can be obtained from the amplitudes of the spherical harmonics at resonance (see Appendix A). Figures 10 and 11 show the evolution of the amplitudes  $\tilde{v}_n$  of the eigenmodes against the normalized frequency  $\omega/\omega_2^{th}$ .

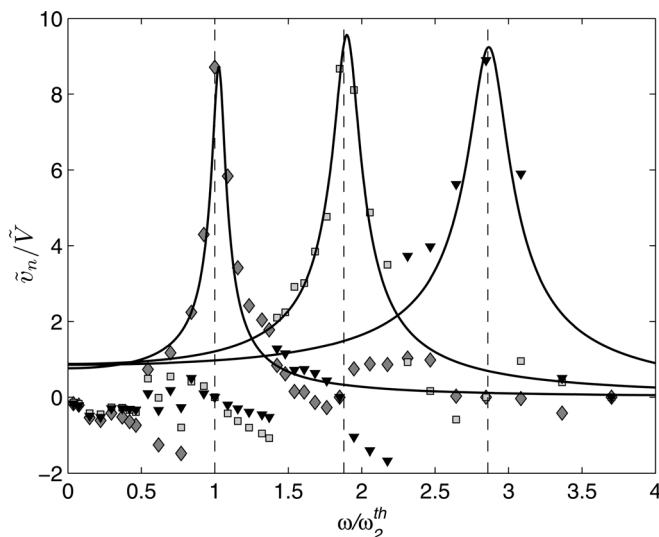


FIG. 10. Amplitudes  $\tilde{v}_n$  of attached modes as a function of the forcing frequency,  $d = 4.19$  mm.  $\diamond$ :  $n = 2$ ,  $\square$ :  $n = 3$ ,  $\nabla$ :  $n = 4$ . The vertical dashed lines mark the theoretical resonance frequencies  $\omega_n^{th}$ .

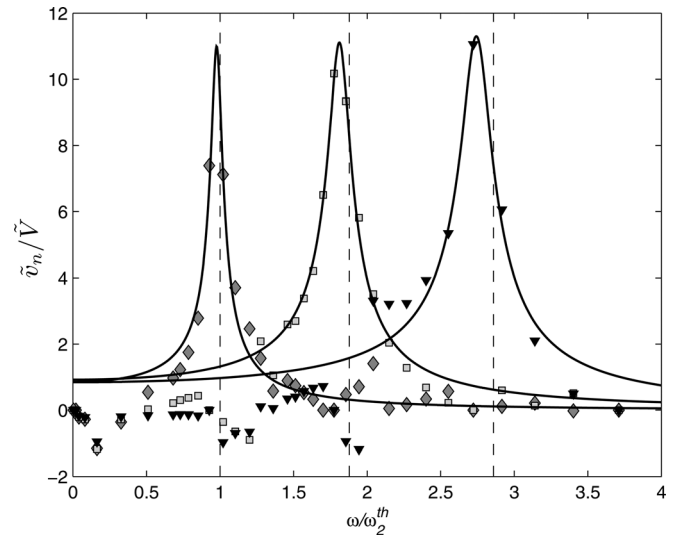


FIG. 11. Amplitudes  $\tilde{v}_n$  of attached modes as a function of the forcing frequency,  $d = 4.48$  mm.  $\diamond$ :  $n = 2$ ,  $\square$ :  $n = 3$ ,  $\nabla$ :  $n = 4$ . The vertical dashed lines mark the theoretical resonance frequencies  $\omega_n^{th}$ .

Eigenvectors are well described by a linear combination of one dominant and several secondary spherical harmonics. Since the resonance frequencies are in good agreement with those of a free drop, dynamics of attached modes is driven by the dominant spherical harmonics. Expressing the shape of the drop in the natural basis of the attached modes does not change the location of the resonance peak and is thus of little interest with regard to the determination of the eigenfrequencies. However, it is necessary to measure with reasonable accuracy the damping rate of each mode, which is a very sensitive parameter to the shape of the resonance curve since it depends on the span-to-height ratio of the peak.

In the linear domain, each eigenmode of the drop shape can be described as an independent linear oscillator. In the oscillatory forced regime, the instantaneous amplitude  $v_n$  of the mode  $n$  is solution of the following differential equation,

$$\ddot{v}_n + 2\beta_n^{exp}\dot{v}_n + (\omega_n^{exp})^2 v_n = F_n \cos(\omega t), \quad (18)$$

where  $\omega_n^{exp}$  and  $\beta_n^{exp}$  are, respectively, the experimental eigenfrequency and the damping rate of the attached mode  $n$ ,  $F_n$  is the forcing amplitude and  $\omega$  the forcing frequency. The general solution of Eq. (18) is given by

$$v_n(t) = \tilde{v}_n \cos(\omega t + \varphi_n). \quad (19)$$

For a weakly damped oscillator, ( $\beta_{exp}/\omega_{exp} \ll 1$ ),  $\tilde{v}_n$  can be written as<sup>26</sup>

$$\tilde{v}_n(\omega) = \frac{2\beta_n^{exp}\omega_n^{exp}\tilde{v}_n^{max}}{\sqrt{(\omega_n^{exp2} - \omega^2)^2 + 4\beta_n^{exp2}\omega_n^{exp2}}}, \quad (20)$$

where  $\tilde{v}_n^{max} = F_n/(2\beta_n^{exp}\omega_n^{exp})$  is the maximum amplitude at resonance. The amplitude  $\tilde{v}_n(\omega)$  of each attached eigenmode therefore depends on three parameters,  $\omega_n^{exp}$ ,  $\beta_n^{exp}$ , and  $\tilde{v}_n^{max}$ , which are determined by fitting the experimental resonance curves with the analytic solution (20) using a least square method. The resonance curves of the three first eigenmodes

TABLE IV. Experimental and theoretical eigenfrequencies and damping rates,  $d = 4.19$  mm.

$n$	$Re_{d,2}$	$\omega_n^{exp}/2\pi$ (Hz)	$\omega_n^{th}/2\pi$ (Hz)	$\beta_n^{exp}$ (s <sup>-1</sup> )	$\beta_n^{th}$ (s <sup>-1</sup> ), Eq. (4)			$\beta_n^{ath}$ (s <sup>-1</sup> ) Eq. (22)
					Potential flow	Boundary layer	Total	
2	1345	27.8	27.0	7.6	0.7	4.6	5.3	6.83
3	2527	51.4	50.8	14.9	1.3	8.7	10.0	11.32
4	3849	77.6	77.2	22.6	2.0	13.7	15.7	15.42

are represented by the continuous lines in Figs. 10 ( $d = 4.19$  mm) and 11 ( $d = 4.48$  mm). The model fitting gives access to the experimental damping rates and allows a more accurate determination of experimental eigenfrequencies. Experimental values of eigenfrequency and damping rate are then compared to those predicted by the linear theory, respectively, in Tables IV and V. As aforementioned, eigenfrequencies of the two largest drops are well predicted by the theory for free oscillating drops, with a maximum error of 3%. Damping rates are systematically underestimated by the free oscillating drop theory. For every  $n$ , the relative difference  $(\beta_n^{exp} - \beta_n^{th})/\beta_n^{exp}$  is about 30% for  $d = 4.19$  mm and 20% for  $d = 4.48$  mm. It is also worth noting that, for both diameters, the experimental and theoretical ratios  $\beta_{n+1}/\beta_n$  between the damping rate of two consecutive modes are approximately the same. This suggests that the discrepancy between experimental and theoretical results comes from the differences between attached and free oscillating drop modes.

Theoretical values for the damping rates of the attached modes are not available for the present configuration. However, they can be estimated by considering that  $\mathbf{V}_n$  vectors are a linear combination of  $\mathbf{Y}_n$ . In the linear regime, the total mechanical energy  $E_n^a$  associated to the attached mode  $n$  (respectively, the dissipation rate  $\epsilon_n^a$ ) is the sum of the total mechanical energies  $E_p$  (respectively, the dissipations  $\epsilon_p$ ) associated to each spherical harmonics with an amplitude  $\tilde{A}_p(\omega_n)$ . Assuming that the damping is weak,  $E_p$  can be considered as constant during a period of oscillation and approximated by the value obtained assuming that the flow is potential,

$$E_p(\omega_n) = \tilde{A}_p^2(\omega_n) \left\{ 2\pi\omega_p^2\alpha^5 \frac{p\rho_c + (p+1)\rho_d}{2p(p+1)(2p+1)} \right\}. \quad (21)$$

By definition, the damping rate is the ratio of the dissipation to the total mechanical energy. The damping rate of attached mode  $n$  can therefore be approximated by,

$$\beta_n^{ath} = \frac{\sum_{p=2}^N \beta_p^{th} E_p(\omega_n)}{\sum_{i=2}^N E_p(\omega_n)}. \quad (22)$$

TABLE V. Experimental and theoretical eigenfrequencies and damping rates,  $d = 4.48$  mm.

$n$	$Re_{d,2}$	$\omega_n^{exp}/2\pi$ (Hz)	$\omega_n^{th}/2\pi$ (Hz)	$\beta_n^{exp}$ (s <sup>-1</sup> )	$\beta_n^{th}$ (s <sup>-1</sup> ), Eq. (4)			$\beta_n^{ath}$ (s <sup>-1</sup> ) Eq. (22)
					Potential flow	Boundary layer	Total	
2	1390	24.1	24.5	5.85	0.6	4.1	4.7	5.55
3	2612	44.5	46.0	11.6	1.1	7.8	8.9	9.33
4	3978	67.9	70.0	15.8	1.7	12.3	14.0	13.81

Tables IV and V report the values of  $\beta_n^{ath}$ , which have been calculated with  $N=5$  by using experimental amplitudes  $\tilde{A}_p(\omega_n)$  reported in Tables VII and VIII. Accounting for the contribution of secondary spherical harmonics significantly improves the agreement with the experimental values of the damping rate of mode 2:  $(\beta_2^{exp} - \beta_2^{ath})/\beta_2^{exp}$  equals 10% for  $d = 4.19$  mm and 5% for  $d = 4.48$  mm. The same tendency, but with a weaker effect, is observed for  $n=3$  while no improvement is obtained for  $n=4$ , which suggests that the contribution of higher order modes ( $N > 5$ ) cannot be ignored for the damping of modes with  $n \geq 3$ . In all cases, the contribution of secondary spherical harmonics seems sufficient to explain the discrepancies observed with the case of a free drop in the absence of gravity.

Another possible cause of discrepancy might be the presence of surface active contaminants that adsorb on the drop interface and tend to increase the viscous dissipation within the boundary layers. This cause has been invoked in the literature<sup>15,16</sup> to explain the disagreement between theory and experimental results. However, it is unlikely that surfactants may affect the damping rate independently of the mode order as it is observed here. It is neither expected that the action of contaminants could increase the damping rate to such a large extent when the drop diameter is just decreased from 4.48 mm to 4.19 mm.

Contribution of secondary spherical harmonics to the eigenmodes of the present attached drops is thus probably the major reason for the observed moderate enhancement of the damping rate. The approximate model accounting for this effect significantly improves the theoretical prediction of the damping rate of mode 2. Moreover, this interpretation is consistent with the fact that the discrepancy is smaller for the largest drop, the eigenmodes of which are closer to those of a free drop.

#### IV. CONCLUSION

Shape oscillations of a buoyant drop attached to a capillary tip have been excited by imposing incompressible sinusoidal volume variations. By considering drops of a few millimeters, a common high-speed camera able to work at 2000 frames per second is sufficient to get an accurate



description of the drop shape up to the frequency of the 5th oscillation mode. Then, the decomposition of the shape into spherical harmonics leads to a comprehensive description of shape oscillations within the linear regime.

Compared to levitation experiments, the present experimental setup is rather simple and easy to operate. However, the investigated case was *a priori* not elementary. First, the drop attachment induced a translational mode and a coupling between the different spherical harmonics. Second, the non-negligible effect of gravity was responsible of a significant drop shape deformation at rest. Also, contaminants were shown to be present.

Surprisingly, provided the Bond number was large enough for a neck to develop at the junction with the capillary, oscillations around a non-spherical shape were found to be close to those predicted for a free neutrally buoyant drop. For the largest drop diameter investigated, measured frequencies of modes  $n = 2, 3$ , and 4 match the theoretical values of a free oscillating drop within 3% while corresponding damping rates are just larger of about 20%. Eigenmodes of the shape oscillations have been expressed as a linear combination of spherical harmonics. Accounting for the effect of secondary spherical harmonics turns out to be sufficient to explain the moderate increase of the damping rate.

A conclusion of practical interest is that the range of validity of the theory derived for a free neutrally buoyant drop is far more extended than expected. In particular, it remains a useful tool to interpret measurements in the present configuration. Then, by adjusting the size of the drop to the density difference, the present method should be adequate to determine the interface dynamics of drops for many liquid-liquid systems, in particular multi-component ones like water in crude oil. The frequency and damping rate measured by the present method could thus be used to predict the breakup occurrence of drops having complex interfaces in turbulent dispersed flows.

## ACKNOWLEDGMENTS

Authors would like to thank Jirí Vejražka from the *Institute of Chemical Process Fundamentals (Academy of Sciences of the Czech Republic)* and Christine Dalmazzone and Christine Noïk from *IFP - Energies Nouvelles* for the fruitful discussions that took place around this work. Jirí Vejražka is also acknowledged for his valuable contribution in the image processing.

## APPENDIX A: DETERMINATION OF THE ATTACHED DROP EIGENMODES

For the two largest drops, the response of each spherical harmonics  $Y_n$  shows a resonance peak at the eigenfrequency  $\omega_n^{th}$  of mode  $n$  of a free drop. However, even if their amplitudes are lower, other harmonics are also present at resonance. It is thus reasonable to assume that in the present case, the eigenvectors  $\mathbf{V}_n$  which form the natural basis for the description of the vibration of an attached drop are linear combinations of the spherical harmonics  $\mathbf{Y}_n$ ,

$$\mathbf{V}_n = \sum_{p=2}^N M_{np} \mathbf{Y}_p. \quad (\text{A1})$$

TABLE VI. Decomposition of shape variations into spherical harmonics at resonance, for  $d = 3.6$  mm.

	$n = 2$	$n = 3$	$n = 4$
$\tilde{A}_2^{alg}(\omega_n)/\tilde{V}$	4.33	2.34	0.29
$\tilde{A}_3^{alg}(\omega_n)/\tilde{V}$	-3.96	4.90	1.09
$\tilde{A}_4^{alg}(\omega_n)/\tilde{V}$	-1.28	-6.63	2.52
$\tilde{A}_5^{alg}(\omega_n)/\tilde{V}$	-1.11	-1.72	-3.84

In order to determine  $M_{np}$ , let us start by the projection of the drop shape variations  $\Delta r$  onto the spherical harmonic basis,

$$\Delta r = a \left( \sum_{p=2}^N \tilde{A}_p \cos(\omega t + \varphi_p) Y_p(\theta) \right). \quad (\text{A2})$$

At the resonance frequency  $\omega_n$  of the  $n^{th}$  mode,  $\varphi_n = \pm\pi/2$  and

$$\Delta r(\omega_n) = a \sin(\omega_n t) \left( \sum_{p=2}^N \tilde{A}_p^{alg}(\omega_n) Y_p(\theta) \right), \quad (\text{A3})$$

where the algebraic amplitudes  $\tilde{A}_p^{alg}$  are equal to  $\tilde{A}_p$  when  $\varphi_n = +\pi/2$  and to  $-\tilde{A}_p$  when  $\varphi_n = -\pi/2$ . Since the resonance peaks are narrow compared to their separation, we can consider that shape oscillations are described by a single mode at each resonance frequency. We can thus determine each  $\mathbf{V}_n$  from the measured shape at the corresponding resonance. From Eq. (A3), we thus get

$$M_{np} = \tilde{A}_p^{alg}(\omega_n) / \left[ \sum_{p=2}^N \tilde{A}_p^{alg^2}(\omega_n) \right]^{1/2}. \quad (\text{A4})$$

Now, it is possible to express the drop shape oscillations at any forcing frequency  $\omega$  in this new basis,

$$\sum_{n=2}^N \tilde{v}_n(\omega) \mathbf{V}_n = \sum_{p=2}^N \tilde{A}_p^{alg}(\omega) \mathbf{Y}_p. \quad (\text{A5})$$

Let  $M_{np}^{-1}$  be the coefficients of the inverse of the matrix  $M_{np}$ , such that  $\mathbf{Y}_p = \sum_{n=2}^N M_{np}^{-1} \mathbf{V}_n$ . The amplitudes of the eigenmodes of the attached drop finally write

$$\tilde{v}_n(\omega) = \sum_{p=2}^N \tilde{A}_p^{alg}(\omega) M_{np}^{-1}. \quad (\text{A6})$$

The  $M_{np}$  coefficients, which are the coordinates of the eigenvectors  $\mathbf{V}_n$ , are deduced from the algebraic amplitudes

TABLE VII. Decomposition of shape variations into spherical harmonics at resonance, for  $d = 4.19$  mm.

	$n = 2$	$n = 3$	$n = 4$	$n = 5$
$\tilde{A}_2^{alg}(\omega_n)/\tilde{V}$	7.82	1.96	0.52	0.52
$\tilde{A}_3^{alg}(\omega_n)/\tilde{V}$	3.43	7.92	2.11	0.90
$\tilde{A}_4^{alg}(\omega_n)/\tilde{V}$	-1.12	-3.98	7.86	1.75
$\tilde{A}_5^{alg}(\omega_n)/\tilde{V}$	-1.29	-1.19	-3.59	7.14

TABLE VIII. Decomposition of shape variations into spherical harmonics at resonance, for  $d = 4.48$  mm.

	$n = 2$	$n = 3$	$n = 4$	$n = 5$
$\tilde{A}_2^{alg}(\omega_n)/\tilde{V}$	7.07	1.92	-1.19	0.47
$\tilde{A}_3^{alg}(\omega_n)/\tilde{V}$	-2.41	9.80	2.10	-1.20
$\tilde{A}_4^{alg}(\omega_n)/\tilde{V}$	-0.57	-2.85	10.49	1.90
$\tilde{A}_5^{alg}(\omega_n)/\tilde{V}$	-1.02	0.89	-2.50	9.79

at resonance provided in Tables VII and VIII by using Eq. (A4). The experimental data corresponding to the two largest drops have been processed by setting  $N = 5$ . Figures 10 and 11 show the evolution of the amplitudes  $\tilde{v}_n$  of the eigenmodes against  $\omega/\omega_2^{th}$ . The representation is here limited to the three first eigenmodes ( $n = 2, 3$ , and 4) because of the lack of resolution of mode  $n = 5$ . Determination of the mode  $n = 5$  with a reasonable accuracy would require to detect the resonance of mode  $n = 6$  in order to extend the series up to  $N = 6$ , which would be only possible with a higher temporal resolution of the video frame rate. Compared to the evolutions of the amplitudes of the spherical harmonics (Figs. 8 and 9), the weight of the secondary modes is significantly reduced, which causes a slight sharpening of the peaks at resonance.

<sup>1</sup>F. Risso and J. Fabre, "Oscillation and breakup of a bubble immersed in a turbulent flow," *J. Fluid Mech.* **372**, 323 (1998).

<sup>2</sup>S. Galinat, F. Risso, O. Masbernat, and P. Guiraud, "Dynamics of drop breakup in inhomogeneous turbulence at various volume fractions," *J. Fluid Mech.* **578**, 85 (2007).

<sup>3</sup>Lord Rayleigh, "On the capillary phenomena of jets," *Proc. R. Soc. A* **138**, 41 (1879).

<sup>4</sup>H. Lamb, *Hydrodynamics*, 6th ed. (1932), Cambridge University Press.

<sup>5</sup>C. A. Miller and L. E. Scriven, "The oscillations of a fluid droplet immersed in another fluid," *J. Fluid Mech.* **32**, 417 (1968).

<sup>6</sup>A. Prosperetti, "Normal mode analysis for the oscillations of a viscous liquid drop in an immiscible liquid," *J. Mécanique* **19**, 149 (1980).

<sup>7</sup>A. Prosperetti, "Free oscillations of drops and bubbles: the initial-value problem," *J. Fluid Mech.* **19**, 149 (1980).

<sup>8</sup>P.-L. Marston, "Shape oscillation and static deformation of drops and bubbles driven by modulated radiation stress—Theory," *J. Acoust. Soc. Am.* **67**, 27 (1980).

<sup>9</sup>H.-L. Lu and R. E. Apfel, "Shape oscillations of drops in the presence of surfactants," *J. Fluid Mech.* **222**, 351 (1991).

<sup>10</sup>J. B. Bostwick and P. H. Steen "Capillary oscillations of a constrained liquid drop," *Phys. Fluids* **21**, 32108 (2009).

<sup>11</sup>M. Strani and F. Sabetta, "Free vibrations of a drop in partial contact with a solid support," *J. Fluid. Mech.* **141**, 233 (1984).

<sup>12</sup>M. Strani and F. Sabetta, "Viscous oscillations of a supported drop in an immiscible fluid," *J. Fluid. Mech.* **189**, 397 (1988).

<sup>13</sup>O. Basaran and D. DePaoli, "Nonlinear oscillations of pendant drops," *Phys. Fluids* **6**, 2923 (1994).

<sup>14</sup>P. L. Marston and R. E. Apfel, "Acoustically forced shape oscillation of hydrocarbon drops levitated in water," *J. Colloid Interf. Sci.* **68**, 280 (1978).

<sup>15</sup>E. Trinh, A. Zwern, and T. G. Wang, "An experimental study of small-amplitude drop oscillations in immiscible liquid systems," *J. Fluid Mech.* **115**, 453 (1981).

<sup>16</sup>H.-L. Lu and R. E. Apfel, "Quadrupole oscillations of drops for studying interfacial properties," *J. Colloid Interf. Sci.* **134**, 245 (1990).

<sup>17</sup>C. Bisch, A. Lasek, and H. Rodot, "Hydrodynamic behaviour of spherical semi-free liquid volumes in simulated weightlessness," *J. Theor. Appl.* **1**, 165 (1982).

<sup>18</sup>D.-W. DePaoli, T.-C. Scott, and O. A. Basaran, "Oscillation frequencies of droplets held pendant on a nozzle," *Sep. Sci. Technol.* **27**, 2071 (1992).

<sup>19</sup>D.-W. DePaoli, J. Q. Feng, O. A. Basaran, and T. C. Scott "Hysteresis in forced oscillations of pendant drops," *Phys. Fluids* **7**, 1181 (1995).

<sup>20</sup>B. Vukasinovic, M. K. Smith, and A. Glezer, "Dynamics of a sessile drop in forced vibration," *J. Fluid Mech.* **587**, 395 (2007).

<sup>21</sup>S. Zeppieri, J. Rodriguez, and A. L. Lopez de Ramos, "Interfacial tension of alkane + water systems," *J. Chem. Eng. Data* **46**, 1086 (2001).

<sup>22</sup>N. Otsu, "A threshold selection method from gray-level histograms," *IEEE Trans. Syst. Man Cybern.* **9**, 62 (1979).

<sup>23</sup>K. Moran and J. Czarnecki, "Competitive adsorption of sodium naphthenates and naturally occurring species at water-in-crude oil emulsion droplet surfaces," *Colloids Surf. A* **292**, 87 (2006).

<sup>24</sup>M. Hoorfar and A. W. Neumann, "Recent progress in axisymmetric drop shape analysis," *Adv. Colloid Interface Sci.* **121**, 25 (2006).

<sup>25</sup>S. Hilgenfeldt, D. Lohse, and M. P. Brenner, "Phase diagrams for sonoluminescing bubbles," *Phys. Fluids* **8**, 2808 (1996).

<sup>26</sup>A. Preumont, *Vibrations Alatoires, Analyse Spectrale* (republished in English, Random Vibration and Spectral Analysis (Kluwer, Boston 1994)) (Presses Polytechniques Universitaires Romande, Switzerland, 1990).